Separation, Size Reduction, and Processing of XLPE From Electrical Transmission and Distribution Cable

C. C. WHITE,[†] J. WAGENBLAST,[‡] *and* M. T. SHAW*

Institute of Material Science
University of Connecticut
Storrs, Connecticut 06269-3136

The recycling of power transmission cable insulated with crosslinked PE (XLPE) was investigated by using different methods of separation and reprocessing. Separation was attempted by thermo-chemical, thermo-mechanical and microwave-mechanical means, the latter being the most successful. A mechanism encompassing all of these was formulated. Compression molding, extrusion, and injection molding with and without preheating of the material were also investigated. It was found that by preheating the XLPE and injection molding under high injection pressure, the neat XLPE could be formed into shapes with tensile strengths equal to that of the original insulation. In view of available observations, possible mechanisms for the flow and reconsolidation of XLPE crumb are proposed and discussed.

INTRODUCTION

The recycling and processing of scrap thermoplastic homopolymer resins have received considerable attention over the past few years and much of this work is summarized in two recent reviews (1, 2). These materials, if pure, can be reprocessed with a minimum of effort to produce virgin-like commodity resins. The recycling of homopolymer thermoset or layered thermosets has not received as much attention (2). Thermosets are generally not considered recyclable due to the relative inability to melt process these materials (1, 2). However, the need to develop strategies for the economical reclamation and reprocessing of thermosets has become important, due in part to consumer and legislative pressures.

The subject thermoset for this work was crosslinked polyethylene or XLPE. One abundant source of the scrap thermoset XLPE is wire and cable. The cable employed in electrical power transmission and distribution, currently valued at over $400M dollars per year in the US alone (1), is a major source of scrap olefin-based polymers. As the country updates its electrical infrastructure, scrap power transmission and distribution cable will present a significant disposal concern as well as an economical source of polymer (1). Typically, once a section of cable is removed from operation, it is sent to a specialized reclaimer who chips the entire cable and recovers the metal conductor (copper or aluminum). The remaining material (up to 70% of the total cable) is a mixture of the various polymers and is contaminated with metal residue (1–2%). Currently this material, referred to as wire fluff, is landfilled. To develop applications for the polymeric components of the cable, a cost-effective, reliable, and environmentally sound method would need to be developed to separate cleanly the components of the cable. The neat components would have a much higher material value than the current wire fluff because the reclaimed product would be pure enough for applications without additional separation or cleaning steps.

A significant fraction of the electric power and distribution infrastructure in the US and Canada uses cable similar to that depicted by the cross section in *Fig. 1* (1). Such cables are composed of a central conductor surrounded by a polymeric insulating material, usually crosslinked polyethylene (XLPE). Surrounding the insulation layer is a second metal layer consisting of grounding wires or foils. Separating the insulation from the metal conductors are layers of "semi-con," typically composed of ethylene copolymers (e.g., EVA, EEA) filled with carbon black. For some applications, the whole assembly may be covered with a protective "jacket," often PVC or Hypalon®.

Separating the cable into neat materials is only the first step. As stated earlier, these thermosetting materials are not readily melt-processable, but could be mixed with a thermoplastic to enhance its material properties. For instance, two recent reports (3, 4) have shown that XLPE/HDPE blends can be effectively

---
*To whom correspondence should be addressed.
[†]Current address: NIST, Building 224, Rm B320, Gaithersburg, MD 20899.
[‡]Current address: Bayer Corporation, Köln, Germany.

employed in molding and extrusion applications. If the thermoset is to be used as a polymer extender, issues such as economical size reduction and processing must be addressed.

This paper is divided into three sections: **Separation Methods**, **Size Reduction**, and **Processing**. In the **Separation** section, the mechanics of three different separation techniques are evaluated in terms of the adhesion between the two layers. In the **Size Reduction** section, the energy and costs associated with grinding the insulation (XLPE) are discussed. Finally, an evaluation of the shaping of these neat materials by a variety of methods is presented in the **Processing** section.

To separate the two polymer components of the cable (semi-con and XLPE), the applied force must overcome that due to the adhesion. In addition the applied force must be less than the mechanical strength of either of the two cable components. The logical mode of separation of cable layers would be similar to that used in the peel test. Typically the adhesion between two layers in such a test is discussed in terms of a steady-state energy balance expression such as

$$P(1 + \varepsilon - \cos\theta) = (St + \gamma)w \tag{1}$$

which can be simplified under certain conditions (see Appendix) to

$$P = \gamma w \tag{2}$$

with an areal adhesion energy γ that depends upon rate of peeling as

$$\gamma = \gamma_0 [1 + f(R, T)]. \tag{3}$$

In these equations, P is the force required to separate the two layers; ε is the strain in the flexible adherent due to the peeling force; θ is the angle of peeling; S is the volumetric work of deformation; γ is the work of adhesion per unit area of adherent; t and w are the thickness and width of the adherent, respectively; and γ_0 is the threshold work of adhesion between the two layers at vanishingly low peel rates (5). Previous studies, at high temperatures and very low peeling rates, have estimated γ_0 at very low values, ~20 N/m (20 J/m^2) for most polymeric systems (6, 7). Similar values have been obtained from calculations based on the surface tension of the two materials (8, 9).

By considering the two terms on the right-hand side of *Eq 1* as both temperature-dependent contributions to the peeling force, the latter can be expressed as:

$$P = P_0 [1 + F(R, T)] = P_0 [1 + f(a_T R)]. \tag{4}$$

The non-dimensional function $f(R, T) = f(a_T R)$ ($0 < f < \infty$) depends on the rate of separation, R, and the temperature, T, of the two materials, which are connected via the temperature shift factor a_T. The importance of the analysis is that it suggests that lower peeling rates or higher temperatures will result in lower peeling forces, and that if there is no adhesion the peeling force will be zero.

One factor not considered in this description is the shear stress on the interface between the two components due to differential thermal expansion. As the

Fig. 1. Cross section of test cable (35-kV power distribution cable). The outer ground wires have been removed, and a longitudinal slit has been machined to facilitate removal of the central conductor core. The outer EVA, XLPE insulation, inner EVA and central Al conductor core are all illustrated. Typical manufacturing practice involves chemical crosslinking of all extruded layers in a high-pressure gas-filled tube.
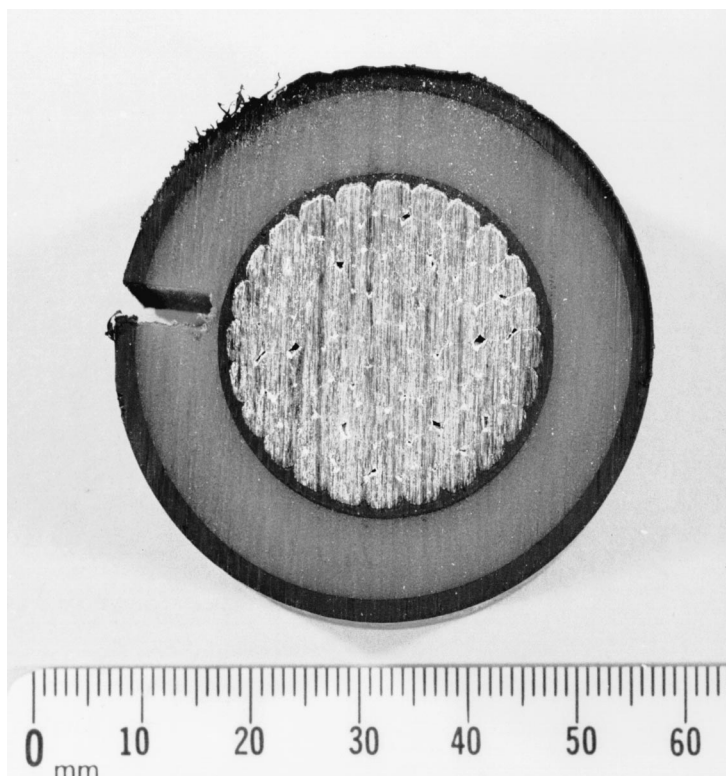
temperature changes, the different thermal expansion coefficients of the two materials will produce a shear stress at the common interface between the two. If this force is large enough, the two materials could separate spontaneously without the presence of an external force. Previous studies in the adhesion literature concentrate on systems where one of the components is flexible and soft and the other component is very rigid. For such a system the contribution from the interfacial shear stress will be very small. In a system composed of two fairly flexible materials, such as the cable system illustrated in *Fig. 1*, this contribution might be significant

While an exact description of the mechanics of the peeling process in the presence of the thermal stress would be desirable, the complexity of the situation dictated a more qualitative approach (see Appendix). To this end experiments were designed to investigate the temperature dependence of the contributions to the peel force, and use these to understand the observed behavior.

EXPERIMENTAL

Material Characterization

The structure of the cable used for all experiments is shown in *Fig. 1*. This 35-kV distribution cable, generously supplied by the Electrical Insulation Research Center of the Institute of Materials Science, University of Connecticut, is very typical of much of the distribution mileage in North America. The inner and outer jacket semi-cons were ethylene vinyl acetate, EVA, filled with carbon black (trade name Semi-Con® from Union Carbide). The 7-mm-thick insulation layer was crosslinked polyethylene (XLPE, HFDA-4201 from Union Carbide; tensile strength of 18.8 MPa; elongation to break 550%). The average molecular weight

between crosslinks was determined by following ASTM D2765. According to this method, sections of known weight of polymer are immersed in a good solvent and allowed to swell. The average molecular weight between crosslinks is determined by the amount of solvent retained in the swollen polymer according to the Flory equation (10).

The gel content was measured separately by the weight loss in the XLPE particles according to ASTM D 2765 using toluene as the solvent modified by the use of a Soxhlet extractor. The gel content of crosslinked virgin HFDE-4201, cured following the protocol obtained from Union Carbide, was 83 ± 1% while the molecular weight between crosslinks from the swelling was 20,600 ± 210 g/mole. (The reported errors represent the 95% confidence limits with three test units cut from three separate plaques, but prepared at the same time.) The measured gel content of the HFDE-4201 for the power transmission cable was 84 ± 2 %, and the molecular weight between crosslinks was 17,000 ± 1,300 g/mole. The tensile properties were measured according to ASTM D638 using an Instron 1101 with pneumatic grips. All test samples were conditioned for 24 h at ambient conditions before testing.

A Polymer Laboratories DMTA Mk II with the tensile head was used to characterize the dynamic viscoelastic properties of the XLPE and EVA samples. The complex modulus (E*) was measured at 1 Hz with a heating rate of 1°C/min for samples of both XLPE and EVA.

DSC Measurement

A differential scanning calorimeter (DSC) was used to characterize the crystallinity of both the EVA and XLPE samples. The DSC used was a TA instruments model DSC 2920; the conditions were a heating rate 10°C/min from 30° to 300°C, with a nitrogen atmosphere. The EVA exhibited two peaks (*Fig. 2*), one peak
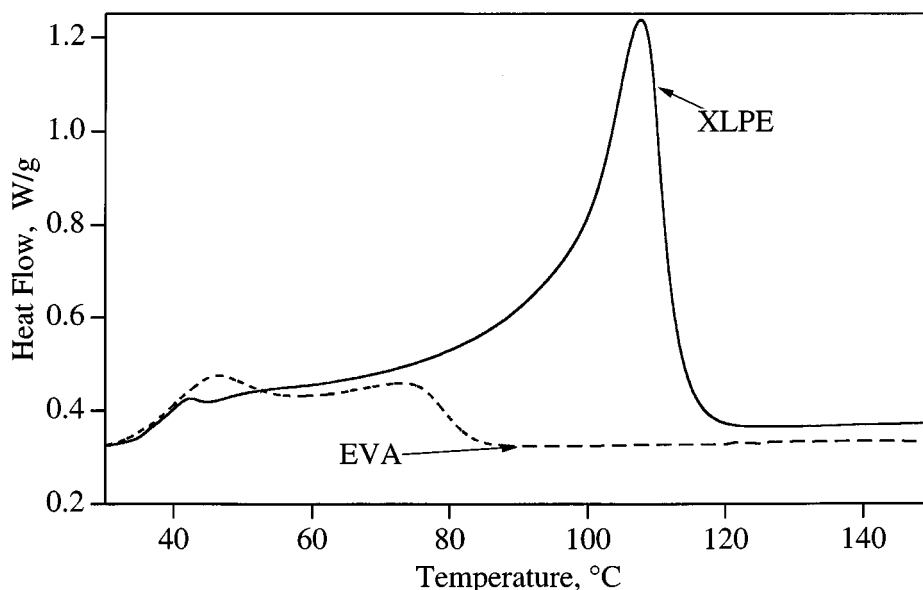

Fig. 2. A differential scanning calorimeter plot of heat flow versus temperature for EVA and XLPE recovered from test cable.

centered at 48°C and the other centered at 74°C. The XLPE exhibited one major peak centered at 110°C. Both EVA and XLPE had similar heat capacities before and after all the crystalline transitions as shown by their similar magnitudes of heat flow when $T >$ 110°C or $T < 50$°C.

Tensile Strength of the Components

While not explicitly included in *Eq 1*, the ultimate tensile strength of the components is clearly an important factor in determining the separability of the two cable components, as this sets the upper limit of the force than can be applied to the sample. To measure the temperature dependence of the ultimate tensile strength of each of the two components, standard ASTM tensile bars were tested at 50 mm/min using an Instron 1101 equipped with an ATS environmental chamber. The specimen, once in place, was allowed to come to thermal equilibrium before testing. Three test units for each material were run at each temperature. The average tensile strengths are shown in *Fig. 3*.

The ultimate tensile strength of the EVA was lower than the corresponding value for XLPE for all temperatures less than ~90°C; above this temperature the XLPE had the lower strength. We conservatively hypothesize that for the XLPE, the steep decline above ~90°C was due to the melting of the crystalline material.

Viscoelastic Properties of Components

The magnitude $|E^*|$ and phase angle (tan δ) values of the complex tensile modulus, E^*, for both XLPE and EVA are shown in *Fig. 4*. The magnitude for EVA is lower than that for XLPE; both exhibited a slight negative temperature dependence. At ~80°C the magnitude of the complex modulus for EVA plateaus

whereas the XLPE value continued to decline, crossing the EVA value at ~110–115°C. With increasing temperature, the XLPE stiffness exhibited a sharp decline from ~110–118°C and then leveled out at a much lower value than EVA.

The tan δ values for both XLPE and EVA were quite low, with EVA having slightly lower values. With increasing temperature, both tan δ values increased with similar slopes, but at 60°C the XLPE values exhibited a pronounced local maximum and started to decrease, crossing the EVA curve at ~75°C. While the EVA tan δ continued to increase, leveling out at ~80°C, the XLPE value consistently decreased until ~110°C, at which point it rose sharply and plateaued slightly below that for EVA.

Although the a_T values (*Eq 4*) for these materials were not measured, they can be estimated from the WLF equation and existing tables of WLF constants (13). Since XLPE has a lower glass transition temperature (–80°C to –130°C) than EVA (~ –25°C) the a_T values calculated from the WLF equation would be lower than the corresponding values calculated for EVA. In addition for each individual component, the a_T value for a given peeling rate/temperature would decrease with increasing temperature. The implication of this observation will be employed in the description of the peeling behavior.

Thermal Expansion Stress

The two components, XLPE and EVA, have different coefficients of thermal expansion (11). As the system is heated from room temperature to 150°C, a measurable thermal stress should result. To estimate its magnitude, direct observations were made of the deflection of long beams of EVA/XLPE as a function of temperature. Assuming these beams behave as elastic
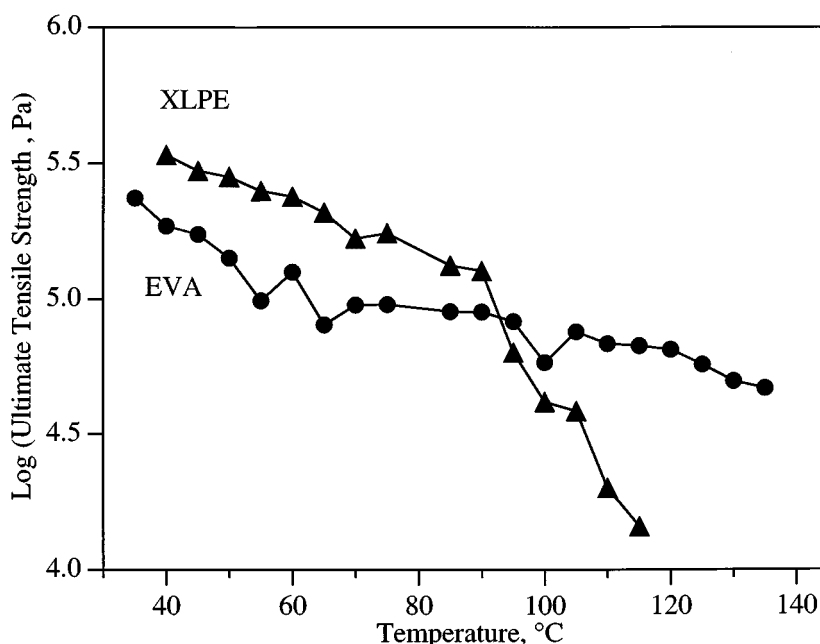

Fig. 3. Ultimate tensile strength of samples of XLPE and EVA tested on an Instron 1101 equipped with an ATS temperature controlled environmental chamber. The points represent the average of three replicate test units.
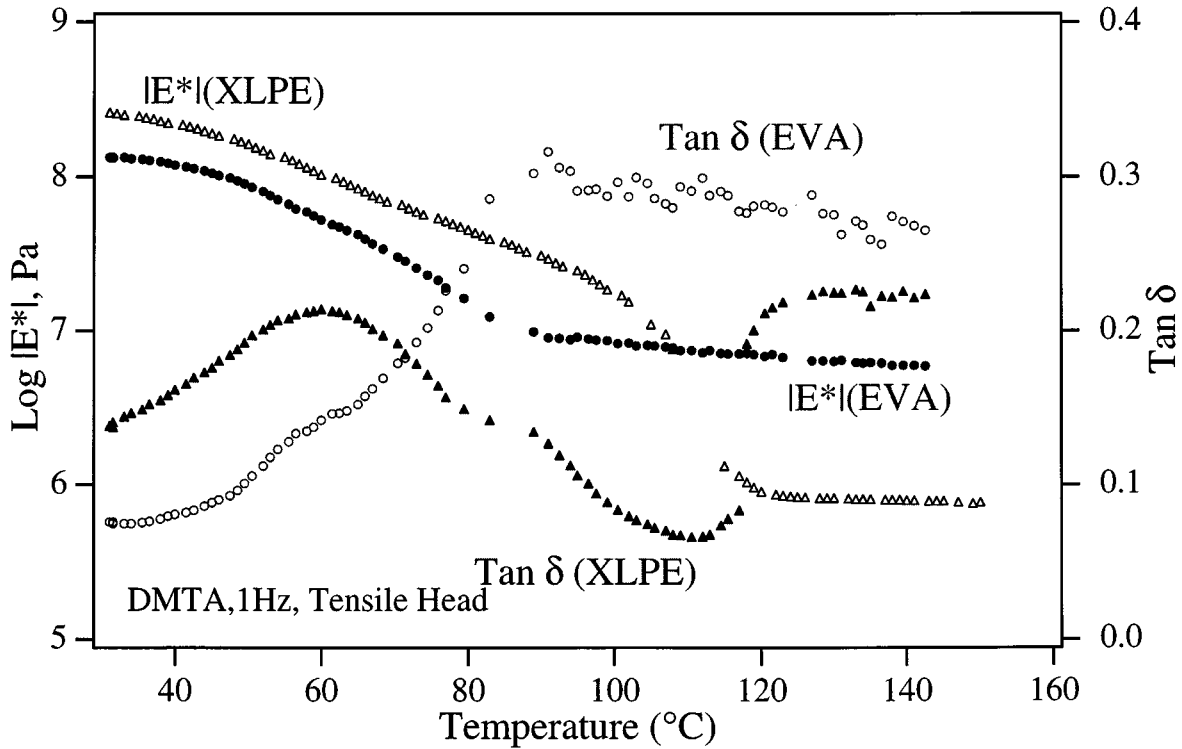
Fig. 4. *The components of the complex tensile modulus, E*, for samples of both EVA and XLPE measured on a polymer laboratories DMTA Mk II with the tensile head. E* was measured at 1 Hz with a heating rate of 1°C/min.*

cantilevers (12), the interfacial shear stress can be estimated from the deflection of the beams at a specific temperature, knowledge of the mechanical properties, and the assumptions of no-slip at the interface between the two materials and no stress relaxation.

The beams were prepared by machining sections from the interface of the power distribution cable. The final beams were 15.24 cm long, 2 mm wide, and 4 mm thick with the thickness evenly divided between the EVA and XLPE. The beams were then hung vertically in a oven. Five thermistors were distributed vertically inside the oven to monitor the temperature along the length of the beams. The temperature of the system was raised at a rate of 0.5°C/min. To determine the degree of deflection, a CCD camera connected to a VCR recorded the entire experiment. Readings from all five thermistors were recorded every 30 s for the duration of the experiment. Images from the VCR consistent in time with the recorded thermistor readings were imported into a computer with a frame grabber. The images were then analyzed for deflection at the end of the beam.

The force, F, required to straighten the beams can be calculated from the apparent deflection

$$F = \frac{4Edwt^3}{L^3}, \qquad (5)$$

where E is the equivalent modulus, d is the deflection, w is the width, t is the thickness, and L is the length of the uniform beam (12) . The equivalent modulus, E,

of a composite beam is presented elsewhere (12), but for the geometry used here, it is simply the average of the two materials. Application of a moment balance (12) gives the thermal expansion stress, τ. This can be calculated from

$$\tau = \frac{F}{A_c} = \frac{4Edt^2}{L^3}, \qquad (6)$$

where A_c is the cross-sectional area of the beam.

The mean values of the equivalent thermal stress for each temperature are presented in *Fig. 5*. Below 60°C, there was no measurable interfacial shear stress. In the range of 60°C < T < 80°C, the shear stress increased with increasing temperature. In this range, the stiffer XLPE should be pushing the softer EVA in the free cantilever. Above 80°C and below ~100°C the stress remained roughly constant at a value of ~10^5 Pa. Above this temperature, the stress decreased with increasing temperature and went to zero. At ~110–120°C, the beam bent back to zero and then started bending in the opposite direction, implying that the stiffer EVA was pushing the softer XLPE. The stress continued to increase up to about 125°C, but reached a value of only ~10^2 Pa.

Peel Experiments

Peel tests were performed on precision machined samples of EVA/XLPE cut from the interface of the power transmission cable previously described. The samples were 8 cm long and 1.27 cm wide. The total
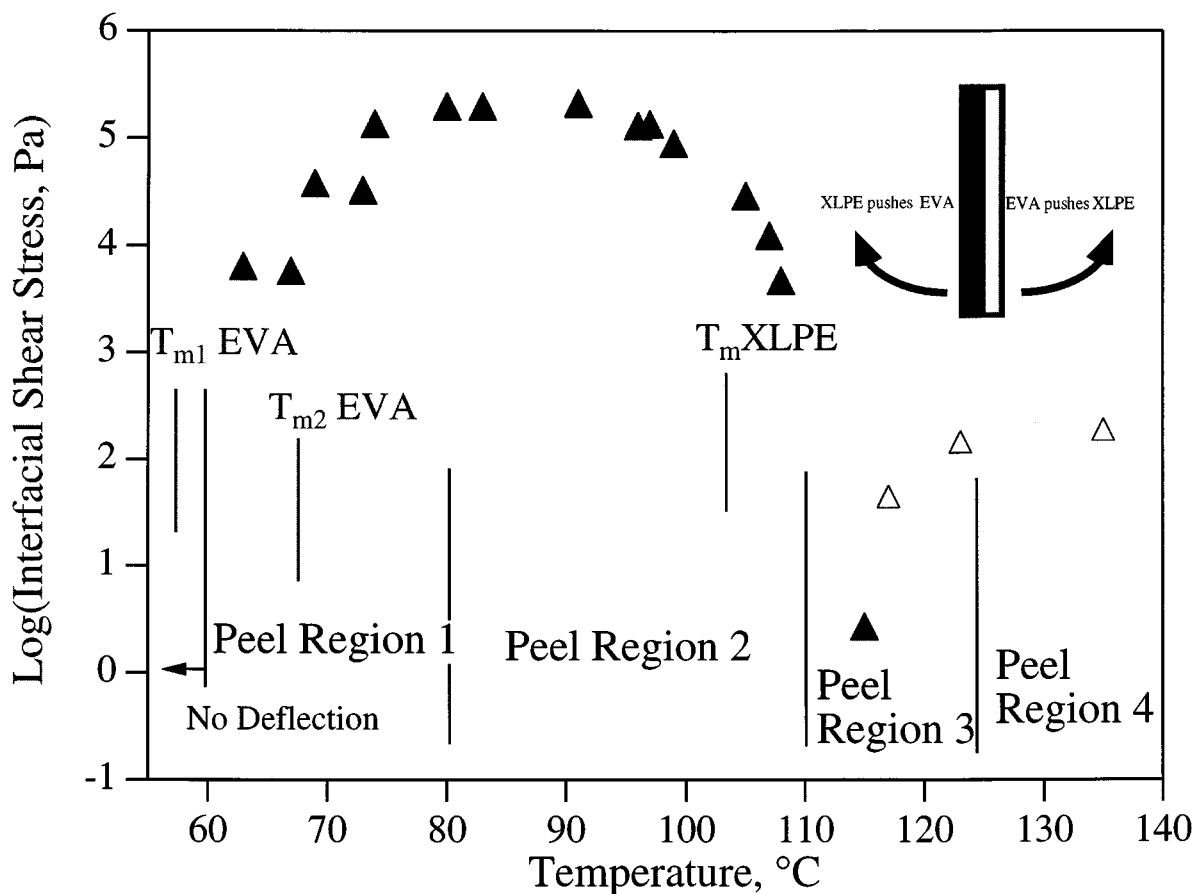
Fig. 5. Thermal expansion stress versus temperature, calculated using Eq 6. The solid symbols represent XLPE pushing the EVA, and the hollow symbols represent the EVA pushing the XLPE.

thickness of 4 mm was made up of two, 2-mm layers of each component. One end of these samples was separated at the interface with a razor to a length of ~1 cm. The free ends of the sample were secured in the jaws of a Instron 1101 equipped with an ATS temperature-controlled chamber. The sample, once in place, was allowed to come to thermal equilibrium. There was no observed difference in the force curve when placing the sample with the XLPE side up or down at each temperature. Once at thermal equilibrium, the cross-head was moved at 50 mm/min. Representative traces of the force versus time (distance) for each of the temperatures are shown in *Fig. 6*.

Four regimes of peeling behavior were observed. At $T < 80°C$ and $T > 125°C$ the force response (*Fig. 6*) showed a sharp rise in the first few seconds of cross-head travel followed by a sharp drop. The onset of this force drop corresponded with the observation of a cohesive failure of the material. At the low temperature this failure always occurred in the EVA, while at high temperatures the failure always occurred in the XLPE. No peeling was evident for this type of behavior. At $80°C < T < 110°C$ there was still a rise in the force, but this was followed by a long region of constant force, the magnitude of which decreased with increasing

temperature. Peeling of the two components was evident at these temperatures, and the unpeeled sandwich was observed to bend towards the EVA side, implying that the XLPE was stiffer than the EVA. For temperatures $110°C < T < 125°C$ the force response decreased and in some cases was not distinguishable from experimental noise. Peeling of the samples was evident for all of these temperatures. In this region, the samples were observed to bend slightly toward the XLPE side.

From this data, a steady peeling force (the average of three peel tests at each temperature) was estimated and is shown in *Fig. 7*. In the case of failure of either the EVA or XLPE, the maximum force was recorded.

Discussion of Peeling Behavior

The origin of a window of clean peeling behavior with a minimum of externally applied force is of great interest and importance. Such behavior is not only of interest in the recycling of these cable systems, but also in determining a possible failure mechanism of this widely used cable system. An additional interest comes from those involved in the installation and repair of the cable, which involves peeling back the semicon to effect connection. As discussed above, four
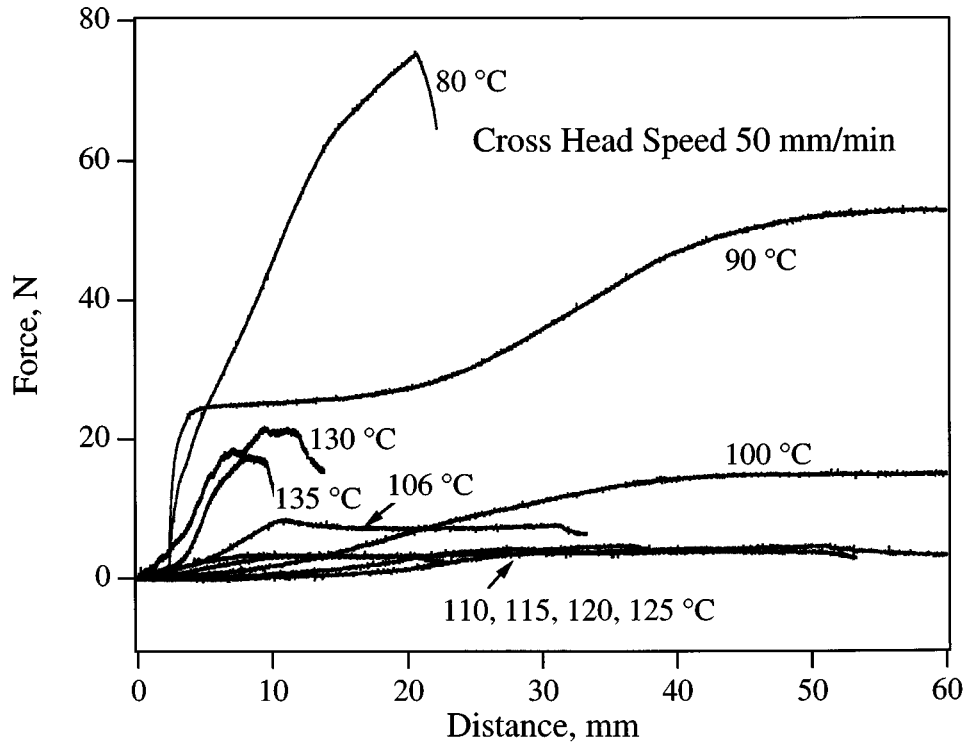
Fig. 6. Representative traces of the force versus time (distance) for each of the temperatures for which peel tests were performed on the EVA/XLPE samples.
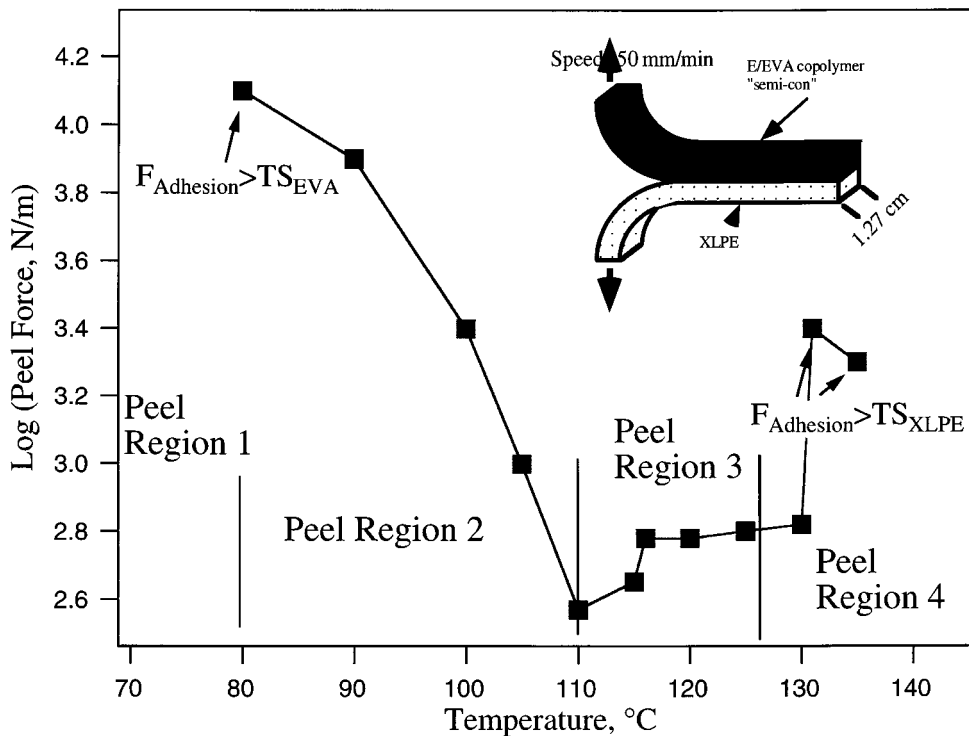

Fig. 7. Peeling force required to achieve steady peel for the EVA/XLPE sample at 50 mm/min as a function of temperature. Each point is the average of tests at each temperature. In the case of failure without peeling, the highest force values were used.

C. C. White, J. Wagenblast, and M. T. Shaw

regions of peeling behavior are present: $T < 80°C$, $80°C < T < 110°C$, $110°C < T < 125°C$, $T >\sim 125°C$. It should be noted that these arbitrary boundaries are valid for the specific peeling rate of 50 mm/min, although the general trends are expected to be similar for other peeling rates.

In the first region, $T < 80°C$, no peeling was evident. In this region, no interfacial stress was evident (bending test) and both materials were strong and stiff (high tensile strength and $|E^*|$). The proposed explanation for this region is that the peel force must not only provide a force per unit width that is greater than the areal adhesion energy (see Appendix), but supply a large amount of plastic work to the substrates as they bend. Greater applied force finally causes the weakest material to fail. At low temperatures this is the EVA.

Both EVA and XLPE have small crystallites containing methylene segments. The EVA has a melting transition in the second peeling regime of $80°C < T < 110°C$. For XLPE, the transition is at slightly higher temperatures (*Fig. 1*); thus, in the range $80°C < T < 110°C$ the XLPE is stiff in comparison to the EVA (*Fig. 4*). The thermal expansion of the XLPE produces a measurable interfacial shear stress (*Fig. 5*). As external force is applied, the softer, more flexible EVA bends at the peel rate tested, giving a conventional peel geometry with a flexible material being peeled from a more rigid substrate. The higher temperature, combined with the differential expansion stress, has lowered the effective work of adhesion to the point where the peeling force is less than the strength of the EVA layer. The magnitude of the steady peeling force decreases with increasing temperature, indicative of a negative temperature dependence of the work of adhesion, as well as a decrease of the effective peeling rate, $f(a_T R)$ in *Eq 4*.

The third region is $110°C < T < 125°C$. In this region the XLPE crystallites are melting (*Fig. 2*) decreasing the stiffness (*Fig. 4*). Under these conditions the filled EVA is the stiffer material and the XLPE peels away from the EVA (the unpeeled strip is observed pointing in the direction of the XLPE). The interfacial stress due to differential expansion is still present, but of a lower magnitude because of the softer materials. The continually dropping work of adhesion is sufficient to permit peeling, even though the tensile strength of the XLPE is dropping rapidly (*Fig. 3*).

In the transition to the fourth region, $T > \sim 125$–$130°C$, the shape of applied force curves were much like those observed for the coldest attempted peels, but of much lower magnitude. We speculate that as the crystallites in the XLPE melt completely, the tan δ value rises, resulting in more lost work, which adds to the peeling force (Appendix). When sufficient force is applied to achieve peeling, the weakest material (XLPE) fails.

The next challenge is to use this knowledge to design and evaluate possible separation methods for the power distribution and transmission cable scrap. Three possible methods were examined: thermo-chemical, thermo-mechanical, and microwave-mechanical.

SEPARATION METHODS

Thermo-Chemical Separation

Ideally, a thermo-chemical separation would involve using the differential swelling power of an appropriate solvent to create a large interfacial shear force that would overcome the interfacial adhesion with minimal externally applied force. This method was originally developed for recycling PVC-covered cables from automotive applications (1). The primary disadvantage of this time-intensive process is the high cost of handling the solvent used in the separation procedure.

To evaluate this method, 1-cm-wide cross sections of the cable were cut to allow diffusion of the solvents into the different regions of the cable in a reasonable time. The inner conductor was removed and the remaining material was placed in either octane at 125°C (boiling point) or decahydronaphthalene at both 120°C and 135°C (195°C boiling point). The amount of time required to separate the two materials was then observed. In the boiling octane or in decahydronaphthalene (decalin) at 120°C, no separation was evident in the cable rings after 1 h of immersion, although there was evidence of swelling of the XLPE layer. For decalin, when the temperature was increased to 135°C, which is above the melting transition of the XLPE, there was clean separation of the components. Heating the cable to this temperature in the absence of solvent, resulted in no cable separation. Octane was proposed as a chemical separation agent as it is inexpensive and its volatility would speed removal of residual solvent. Decalin was evaluated as a good solvent with a higher boiling point (195°C).

This method, while effective at separating the cable components at higher temperatures (135°C), has several drawbacks. It involves long soak times in high-temperature organic solvent and, after separation, the solvent must be completely removed from the recovered materials. Therefore this method was judged to be a cost-prohibitive process for the industrial separation of power distribution and transmission cable.

Thermo-Mechanical Separation

To evaluate this method, slit cable sections (50 cm long) were incubated in a Blue M Stabil-Therm oven at 130°C for 1 h to achieve thermal equilibrium. The cable sections were then removed from the oven and hand-generated mechanical force was applied to them as they cooled. Using this method, the inner, outer and conductor core could easily be separated from the XLPE dielectric. A continuous process for the separation would involve a combination of longitudinal slitting of the polymeric cables, elevated temperature ($\sim 120°C$), and application of a mechanical separating force (*Fig. 8*). With the thermo-mechanical separation of the material, we were able to generate large volumes (on a laboratory scale) of the neat components of the cable.

The thermal-mechanical separation yields cleanly separated components with no metal contamination
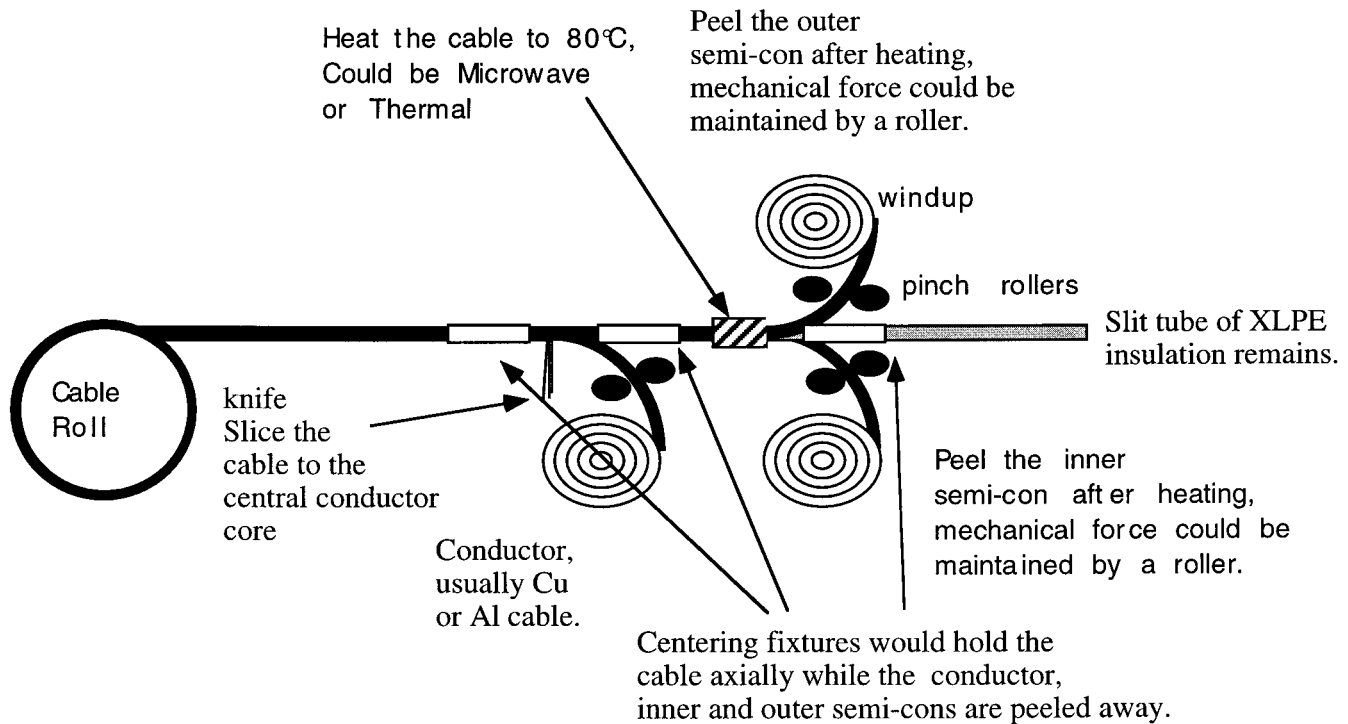
Fig. 8. *Schematic of proposed process for thermal or microwave separation of power cable.*

at a cost that could be lower than the cost of traditional recovery of the cable (chipping and sorting). A disadvantage of this method is the long soak time at elevated temperatures, which would limit line speed and throughput. Optimizing this method would require a method of rapidly and economically heating the cable sections.

Microwave-Mechanical Separation

The use of microwave energy to replace convection heating could provide a method of heating the cable very rapidly without the long soak-times of the thermo-mechanical method, thus increasing throughput. All the microwave experiments were conducted with a Lambda Technologies variable frequency microwave furnace (model LT 502xb). This furnace could vary the principle frequency between 2.5–7 GHz, producing radiation with bandwidth between 1 Hz and 5 GHz (household microwave ovens emit radiation at a single frequency, 2.54 GHz). Forward or input power could also be adjusted.

The use of microwave energy instead of radiant energy has the potential advantage that instead of heating the entire cable, only one of the components is heated, and that component in turn heats the interface between the two components to lower adhesion. Additionally, higher expansion stresses would result. Therefore, the frequency of the microwave furnace should be selected such that only one component of the cable assembly absorbs the radiation. The following equation may be used to describe the power balance in the microwave cavity:

$$P_{Forward} - P_{Re\,flected} = P_{Cavity\ Absorption} + P_{Material\ Absorption} \quad (7)$$

The forward or input power and the reflected power for a whole section of cable is illustrated for the entire microwave range (2.5 GHz to 7 GHz) in *Fig. 9*. Similar curves were obtained for the EVA and the XLPE. The shape of the forward or input power curve is typical for this type of microwave source. The large non-random noise associated with the source is evident from this *Figure*.

For the present system, it proved to be impossible to select a particular frequency at which one component selectively absorbed microwave energy. Part of the problem was variability in the absorption spectrum. This variability not only depends on the character of the cavity, but the placement and geometry of the sample within the cavity. Several different types of subtractions were performed to limit the amount of variability in the spectrum, but all were unsuccessful.

Single-frequency microwave radiation is not uniformly distributed within the cavity. There are two strategies to achieve uniform heating of materials in a microwave cavity: 1) rotate the material within the cavity by physically moving the material through the regions of high and low intensity radiation, or 2) irradiate with a finite bandwidth. With a finite bandwidth, each single frequency would produce localized heating within a specific part of the cavity, and the sum of the intensity of each of the individual frequencies would result in a uniform radiation level within the cavity.

The heating rates for individual components of the cable with constant input microwave energy were
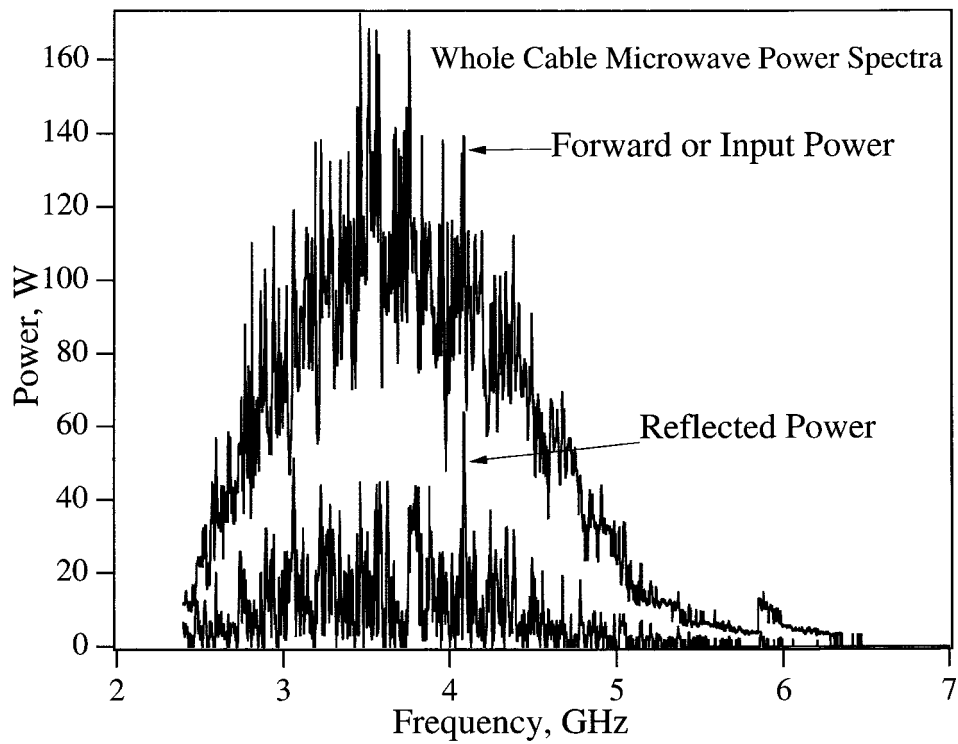
Fig. 9. The forward and reflected power from a Lambda variable frequency microwave furnace from 2.5–7 GHz for a section of whole cable within the cavity of the furnace. The general shape of this curve is typical for this type of microwave source.
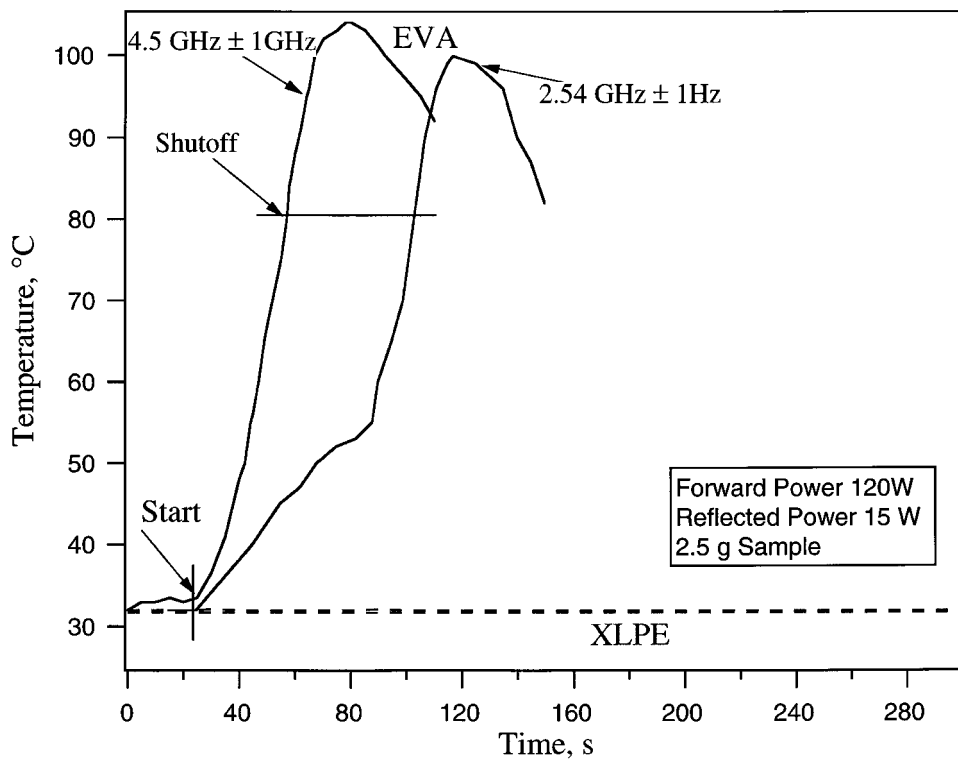

Fig. 10. Microwave heating curves for separate specimens of EVA and XLPE. The EVA absorbs larger amounts of microwave radiation. Two different types of heating—narrow and broadband frequency distributions—are shown for the EVA.

measured for the two different heating regimens (*Fig. 10*). A 2.5 g sample of one of the components was placed into the cavity of the furnace with similar input power in replicate runs, with no adjustments to the settings. The settings used were: 100 W forward power, at either 4.5 GHz with a 1 GHz bandwidth or at 2.54 GHz with a 1 Hz bandwidth, programmed to heat to 80°C and hold for 5 min. Several features were evident. The EVA heated rapidly, while the XLPE did not heat appreciably, resulting in the realization of our objective without requiring a unique separation frequency. When the EVA was heated with a single frequency, the spatial non-homogeneity of the radiation was evident as a temperature-versus-time plot showed two different slopes during heating (*Fig. 10*). These two temperature responses represent a region of high radiation and a region containing the temperature probe that has lower radiation. Temperature measured by the probe will be due initially to absorption of microwave energy in the non-probe end of the material and induction at the probe end of the material. As the non-probe end of the EVA melts it will begin to conduct more heat to the region containing the temperature probe, resulting in an increase in the heating rate measured at the temperature probe. If the radiation source were of a broader bandwidth, the heating rate would be more uniform and rapid.

Under both microwave conditions tested, the EVA was heated above the programmed temperature by ~20°C. One possible reason for this temperature overshoot was deduced from a differential scanning calorimetric trace. In the DSC curves, two endothermic peaks were found (*Fig. 2*). The enthalpy associated with these two peaks, one centered at 48°C and one centered at 74°C, totaled 34 J/g. The specific heat of EVA is 0.4 W/g °C below 80°C, but above 80°C, it drops to 0.2 W/g °C, resulting in rapid heating. Although the power is shut down at 80°C, the recorded temperature continues to rise through heat conduction from the hotter region for a couple of additional seconds. In all the experiments, no appreciable temperature change was evident in the XLPE, as shown in *Fig. 10.*

Due to physical limitations of the microwave cavity, small cable rings similar to those used in the thermochemical separation were placed in the furnace, and the temperature probe was inserted between the outer EVA jacket and the XLPE insulation. The cable was then subjected to an input power of 100 W with a principal frequency of 4.5 GHz and a bandwidth of 1 GHz. The observed heating rate was lower than what was seen for the EVA alone, suggesting that as the EVA was heated by absorption of the microwave radiation, some of that energy was conducted into the XLPE through the interface. It was also observed that the heating rate was widely variable (0.07 to 0.22 °C/s) and not directly related to the mass of the cable (this is due to the large and variable cavity absorption). Based on these experiments, we estimated that the cable absorbs between 3–30% of the total microwave energy. After heating the cable to only 80°C the

outer and inner EVA could be separated from the cable in a process similar to that employed in the thermal-mechanical method. Heating the cable with microwaves required between 0.23 to 2.6 kW h/kg of energy.

Clearly this process was not optimized, and discussions with the manufacturer of the microwave suggested that improvements in the microwave design would yield improvements in both heating rate (process speed) and increased efficiency of several orders of magnitude (~0.02 kW h/kg, ~10 s heating time or better). One possible scheme for separating the cable is shown in *Fig. 8*.

SIZE REDUCTION

To incorporate XLPE into resins for new applications, the XLPE would have to be reduced in size. To investigate this process, the XLPE was ground at both the thermal separation temperature (130°C) and at room temperature in a Wiley Laboratory Mill (model 4) to different particle sizes. The power consumption of the mill was measured using a Weston Wattmeter (ac and dc, model 310). The current flow during the grinding operation was measured using a Amprobe RS-1a ammeter which exploits the magnetic flux density resulting from the current flow. The advertised accuracy of this ammeter is ± 0.2 A. The combination of these two measurements allowed the calculation of a power factor versus current, thus yielding the in-phase power consumed by the mill, as opposed to reactive power. (The former is billed to the customer by the utility.) The resulting particle size distribution was evaluated using standard mesh sieves.

The results of the grinding experiments are shown in *Fig. 11*. For 4-mm XLPE particles ground at ambient conditions, 0.09 kW h/kg was required, compared with 0.07 kW h/kg when the XLPE was heated to 130°C. There was one qualitative difference observed between ambient and preheated ground XLPE. The XLPE ground at ambient conditions had a much more elongated shape, which is consistent with the toughness of the material. At elevated temperatures the XLPE appeared to be cut more cleanly. The specific energy required to grind the XLPE to a particular particle size has a slope of –2 on this log-log graph, which is consistent with the production of new surface area as the main use of the energy. Also included in *Fig. 11* are literature values for two other (larger) grinding operations (15). For grinding polyethylene bottles to 2-mm pieces in a 30-kW Alpine mill (16) and for polyethylene pieces to 2.2 mm in a 30-kW Condex Mill, (17, 18) the reported energy values are similar to those obtained with the Wiley Laboratory Mill in this study. Using an energy cost of $0.05/kWh, the cost associated with grinding the XLPE to a specific particle size was estimated, and is included in *Fig. 11*.

PROCESSING

It has been demonstrated previously that XLPE crumb can be effectively included in thermoplastic
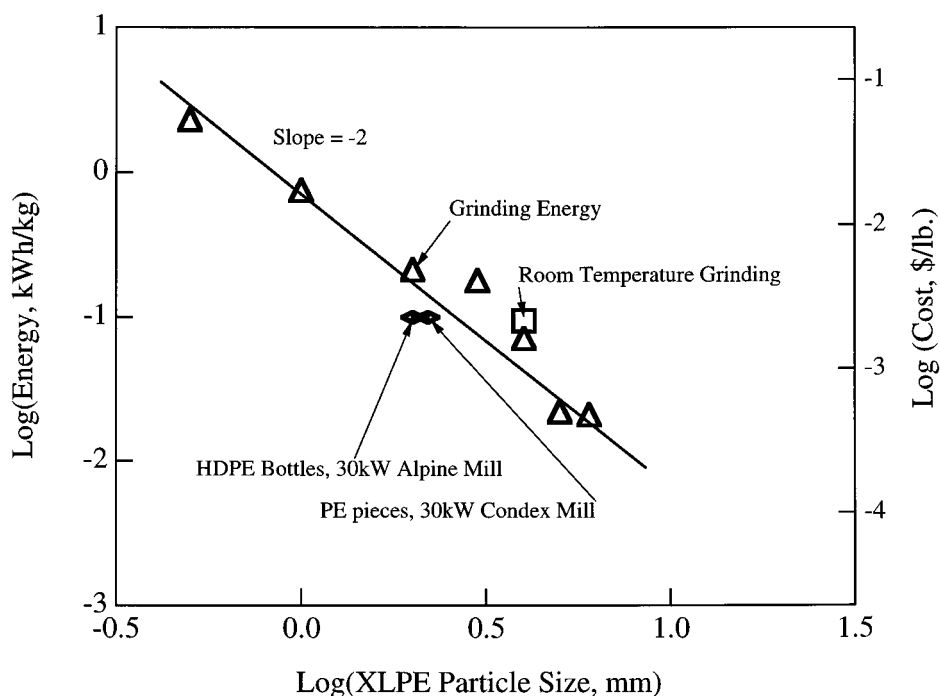
C. C. White, J. Wagenblast, and M. T. Shaw

Fig. 11. Specific grinding energy for XLPE.

blends (3, 4). One additional application to consider is the direct reprocessing of the XLPE crumb. To examine the feasibility of the direct reprocessing of the XLPE crumb, three standard methods were evaluated: compression molding, extrusion, and injection molding.

Compression Molding

In this process, recovered ground XLPE crumb was compression-molded at 180°C and 30,000 lb using a laboratory press (F.S. Carver Inc., Menomonee Falls, WI). The time interval from sample introduction to full pressure was 30 s, with a holding time at full pressure of 120 s. Using this process, the following plaques were prepared: a thicker plaque (21 cm × 21 cm × 0.32 cm) for tensile samples and a thinner one (12.7 cm × 12.7 cm × 0.19 cm) for Environmental Stress Crack Resistance (ESCR) analysis. A control of virgin XLPE was processed using a similar procedure.

The resulting material from this process had poor appearance and properties, although some sintering was observed.

Extrusion

In this process, the ground sieved XLPE crumb (1.2 mm) was fed into a 1-in. single-screw extruder with a barrel temperature of either 140°C or 190°C. In addition to the expected high back pressure and low throughput, the extruded XLPE "melt" exhibited extreme die swell and exited the die as a unconsolidated fluff at both temperatures tested.

Above the melting temperature of the crystals in XLPE, there is considerable chain flexibility, and large deformations of the particles are possible. The

situation results in granular flow with highly elastic grains. Continuous bulk flow is possible by the relative motions of the particles. After passing through the die, the stretched particles reorient under the reduced stress, which produces significant deformation and delamination of the XLPE.

Injection Molding of XLPE Grindings

Two methods of directly reprocessing the recovered XLPE by injection molding were investigated. In the first method, fine (1.2 mm) XLPE crumb was used as a feedstock, and in the second method large chunks were used. The latter were 50 mm × 20 mm × 7 mm, and were the largest pieces that would fit into the throat of the molding machine, an Arburg model 221-75-350. The molded samples obtained in these studies were standard tensile (ASTM 638) and ESCR (ASTM 1693) samples. For the XLPE crumb, the feedstock material was fed into the injection molder at ambient temperature; the maximum injection pressure was 135 MPa and the barrel temperature was 190°C for all zones. For the injection molding of the larger pieces, the XLPE pieces were preheated in an oven at 130°C. Under these conditions, the maximum injection pressure was 110 MPa, and the barrel temperature was 190°C.

Both of these reprocessing methods yielded molded parts composed of relatively homogeneous material. However, the required injection pressure was quite high at 135 MPa and 110 MPa for XLPE crumb and chunks respectively, and the self-induced barrel temperatures reached 250°C and 240°C, respectively. These high pressures and temperatures are the result of the high "viscosity" of the XLPE.

Table 1. Measured Material Properties on Reprocessed Cable Scrap.

Run	Feedstock	Tensile Modulus, MPa	Ultimate Tensile Strength, MPa	Elongation at Break, %
1	XLPE (ambient, ground to 1.2 mm)	180 ± 20	16.2 ± 0.3	44 ± 3
2	XLPE (preheated to 130°C, chunks)	181 ± 20	15.8 ± 0.2	39 ± 3
3	Whole cable (ambient, ground to 1.2 mm)	152 ± 24	9.1 ± 0.2	22 ± 4
4	XLPE, strips from cable (No processing)	203 ± 20	14.3 ± 0.2	477 ± 60

With preheated XLPE, the starting particle size did not influence the injection molding process so long as the particles were able to fit into the channel of the reciprocating screw. This suggests that there is considerable size reduction during the process. Reprocessing of large preheated pieces by injection molding reduces the total energy requirement by eliminating the need to grind the XLPE, and by reducing the energy required to reprocess the material.

An analysis of all the processes suggests that a combination of effects must be present to form mechanically cohesive 100% XLPE materials. In compression molding, elevated temperature and pressure are present, but chain entanglement was inadequate to form mechanically cohesive parts. In the extrusion process, a combination of the elevated temperature and shear stress are present, but the absence of a high-pressure hold results in delamination of the XLPE. It is only during injection molding that all of the process conditions are appropriate to form XLPE parts. While these hypotheses are consistent with our observations, the observations are from tests with limited process conditions and equipment.

Mechanical Properties of Reprocessed XLPE

The tensile bars obtained from the injection molding of the 100% XLPE were tested on the Instron 1101 previously described. Representative stress-strain curves for the reprocessed XLPE parts obtained from injection molding are shown in *Fig. 12*. Two additional sets of data have been included on this plot: (1) the values obtained using bars made by grinding to 1.2 mm and injection molding the whole cable, after removing the Al conductor core and (2) the value obtained from machining standard tensile test parts (ASTM D 638) directly from the "neat" XLPE cable insulation. The results are listed in *Table 1*; they consist of sample averages of ten test units ± the range of values within each sample drawn from one grinding and molding run. The results suggest that we can eliminate the particle size of the XLPE as a factor (Runs 1 & 2). By pooling Runs 1 & 2 and comparing with Run 3, we can argue that freeing the polymeric components of the cable from the copolymer semicon results in an increase in the modulus and ultimate mechanical properties. The results from Run 4, derived from parts machined directly from the undisturbed XLPE insulation,
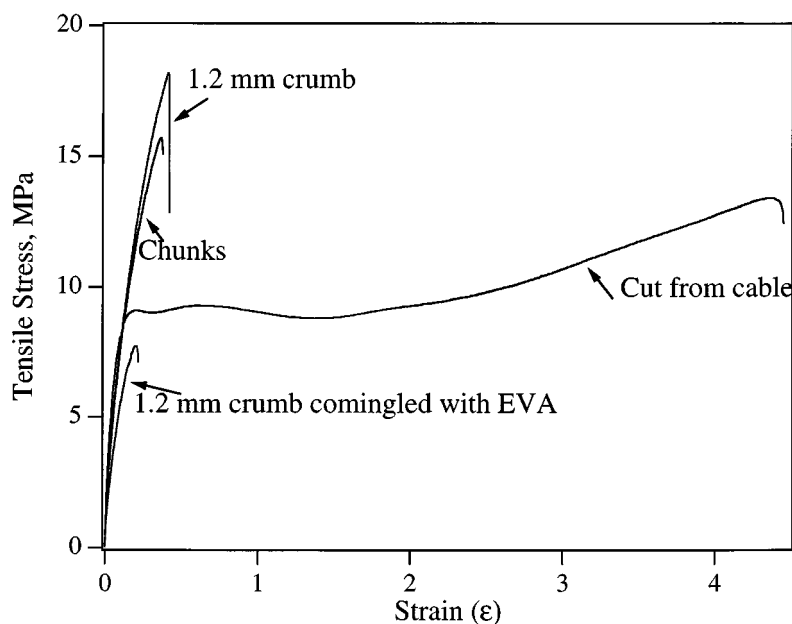

Fig. 12. Stress-strain plot for the XLPE tensile parts prepared through the injection molding process. Also included are stress-strain plots for whole cable (ground and injection molded) and XLPE cut directly from the power cable.

C. C. White, J. Wagenblast, and M. T. Shaw

suggest that the knitting of the XLPE in the injection molding process was far from complete. However, these injection-molded parts could be suitable for some applications requiring solvent resistance.

CONCLUSION

In this paper we have demonstrated that elevated temperature (high enough to melt the crystals, but not high enough to degrade the mechanical strength of the material) in combination with mild mechanical force can effectively separate the components of a typical power distribution cable. This process has a significant advantage over current cable recovery operations in that it produces material that is free of contamination from the other components of the cable.

We have examined the peeling of two viscoelastic components from each other in the context of separating and recovering typical power distribution cable. We have used the components of an EVA/XLPE cable system as a model system to investigate the relative magnitude of the terms in a peeling energy balance. From this analysis we have established four regions: (1) low temperatures ($T < 80°C$), where the peeling force is greater than the ultimate tensile strength of the EVA; (2) intermediate temperatures ($80°C < T < 110°C$), where the softer EVA is peeled away from the XLPE, (3) slightly higher temperatures ($110°C < T < 125°C$) where the softer XLPE is peeled away from the EVA, and (4) higher temperatures ($T > 125°C$) where the required peeling force is greater than the mechanical strength of the XLPE.

This behavior prompted the evaluation of three potential recovery processes: thermo-chemical, thermo-mechanical, and microwave-mechanical. All three methods were successfully used to separate the cable. However, the thermal-chemical method was judged impractical for industrial scale separation due to the requirement of long-time immersion in hot organic solvents. The thermal-mechanical method was effective and had the lowest energy cost of separation (0.16 kW h/kg), but this method also required lengthy heating times (1 h for the 35-kV cable studied). The most promising method of separation involved a rapid heating of the cable by microwave energy, either a single frequency or finite bandwidth, (100 s) followed by

mechanical separation. With standard microwave furnace cavity design, this method required more energy (0.23–2.62 kW h/kg) than heating the entire cable, but changing the cavity design should improve this process both in speed and efficiency (estimated at ~0.02 kW h/kg in 20 s).

The energy required to reduce the size of the XLPE dielectric material has been measured. This information will be useful if the XLPE is incorporated as a polymer extender in other resins. The total energy required to produce particles of *size D* follows the relationship D^{-2} within the size range of 0.5 to 8 mm. The energy required to grind the XLPE was lowered by a factor of 3 if the XLPE was heated to a point where the crystals melted.

Direct reprocessing of the crosslinked XLPE has also been demonstrated. Injection molding was the only method that yielded reasonably sound parts. It was also found that initial XLPE particle size did not seem to be a factor in the measured materials properties.

APPENDIX

In peeling apart a length of insulation L, the peeling force P acts through a distance $L(1 + \varepsilon - \cos\theta)$ where ε is the strain in the strip under the imposed force P. The cosine term takes care of the fact that the line of contact moves backwards as the peel comes off. The energy associated with this work goes into surface forces and peel deformation, as described, for example, by Gent and Hamed (19), with the equation

$$P(1 + \varepsilon - \cos\theta) = (St + \gamma)w, \tag{A1}$$

where S is the volumetric energy due to deformation of the peel, and γ is the areal work of adhesion. The geometric variables are given in *Fig. A1*. If the peel angle is 90° and tape is elastic, the solution is

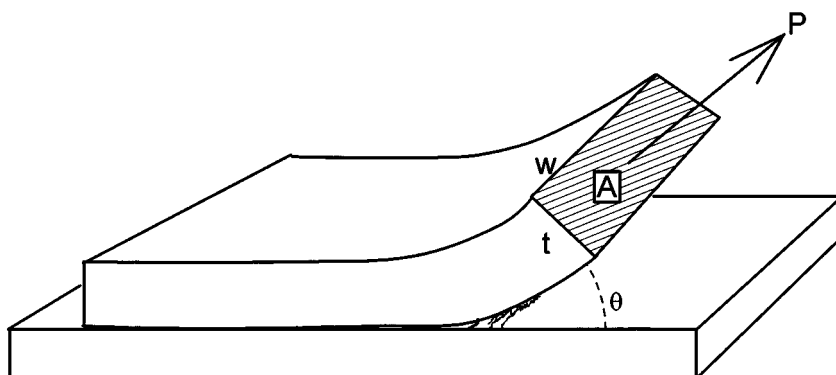$$\widetilde{P} = -1 + \sqrt{1 + 2\widetilde{\gamma}}, \tag{A2}$$

where $\widetilde{P}$ is the reduced peeling force given by

$$\widetilde{P} = P/AE, \tag{A3}$$

and $\widetilde{\gamma}$ is the reduced surface energy given by

$$\widetilde{\gamma} = \gamma/Et. \tag{A4}$$

Fig. A1. Peeling a viscoelastic solid.

In these equations, E is the Young's modulus of the peel.

As the surface energy term combines both thermodynamic and viscoelastic contributions, it is expected to depend on peeling rate. If the peeling angle is nonzero, material lying flat on the stiff substrate is bent, straightened and stretched. There is no consequence of this complex deformation if the material is elastic; however, a viscoelastic material will heat up.

To estimate the qualitative effect of viscous loss, the material was first assumed to be a Voigt solid, with the tensile response given by:

$$E(t) = E$$

$$E' = E$$

$$E'' = \omega\eta$$

$$\tan\delta = \omega\eta/E \qquad (A5)$$

where E and η are the characteristic parameters elastic and viscous elements of the Voigt solid and ω is the frequency (13). Clearly the peel is not a simple Voigt element, but it is reasonable to suppose that the qualitative effects will be similar.

If the undeformed peel is suddenly subjected to a constant peeling force P, it will deform according to the equation

$$\varepsilon = \frac{P/A}{E}\left(1 - e^{-t/\tau}\right) \qquad (A6)$$

where A is the cross-sectional area of the peeling strip and $\tau = \eta/E$. The total specific energy S required by this deformation will be

$$S = \frac{P\varepsilon}{A} = \frac{P^2}{E'A^2} \qquad (A6)$$

For a Voigt element, the stored energy is always 1/2 of this value and thus is equal to the energy stored in an elastic system, i.e.,

$$\tfrac{1}{2}E\varepsilon^2 = \tfrac{1}{2}(E\varepsilon)\varepsilon = \tfrac{1}{2}\sigma\varepsilon = \tfrac{1}{2}\frac{P}{A}\varepsilon \qquad (A8)$$

where σ is the stress at strain ε.

The first law, $U = Q-W$ applied to the isothermal transient peeling of a length of tape suggests that the increase in internal energy will comprise the increase in surface energy and stored elastic energy.

For an elastic system, this is simply the equation of Anderson *et al.* (20).

$$\frac{P(1 + \varepsilon - \cos\theta)}{A} = \gamma/t + \tfrac{1}{2}\frac{P\varepsilon}{A} \qquad (A9)$$

because no heat is involved and the stored energy in the elastic material is given by *Eq A8*.

For a Voigt element, the stored energy is the same as the elastic material, but the dissipated energy is lost as heat to the surroundings (isothermal process). The net result of this for the Voigt element is:

$$\frac{P(1 + \varepsilon - \cos\theta)}{A} = \gamma/t + \frac{P\varepsilon}{A} \qquad (A10)$$

where the second term on the right is the total deformation energy of the Voigt element. The simplification of this for a constant-force deformation of a Voigt substrate in peeling is

$$P = \frac{A\gamma}{t(1 - \cos\theta)} = \frac{w\gamma}{1 - \cos\theta} \qquad (A11)$$

as if the peeling strip had not stretched at all. If the peel angle is 90°, $P = w\gamma$, which is *Eq 2* in the Introduction.

What appears to be illogical is the fact that the constant-force deformation of the Voigt element never approaches the elastic element no matter how insignificant the viscous part of the Voigt element. This stems from the problem of stretching an elastic material at constant force. This can be avoided by considering a three-element solid comprising a Voigt element in series with an elastic element (21). This analog, depicted in *Fig. A1*, has the viscoelastic properties:

$$\tan\delta = \frac{\omega\tau}{[1 + (\omega\tau)^2]/\widetilde{E} + (\omega\tau)^2} \qquad (A12)$$

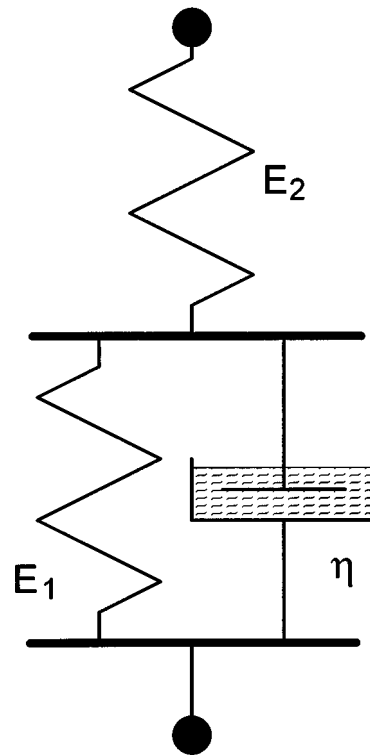$$E' = E_e\left(1 + \widetilde{E}\,\frac{(\omega\tau)^2}{1 + (\omega\tau)^2}\right) \qquad (A13)$$

Fig. A2. Solid analog used for calculating tape peel properties.
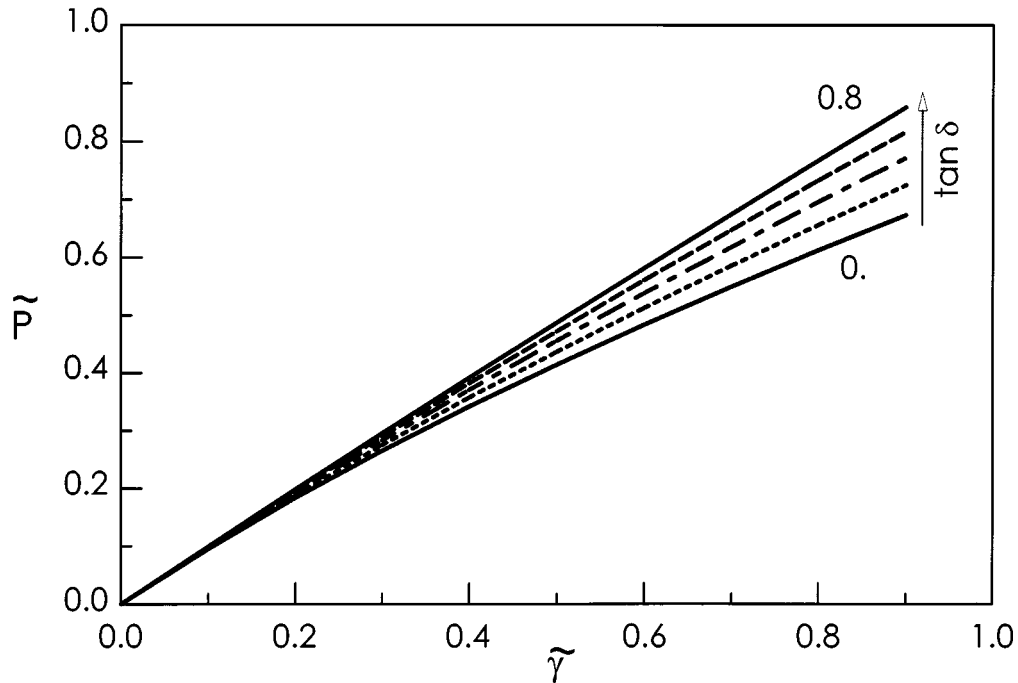
C. C. White, J. Wagenblast, and M. T. Shaw

Fig. A3. Influence of loss tangent on peel force.

$$E'' = E_e \widetilde{E} \frac{\omega\tau}{1 + (\omega\tau)^2} \qquad (A14)$$

where

$$\widetilde{E} = E_2/E_1 \qquad (A15)$$

$$\tau = \eta/(E_1 + E_2) \qquad (A16)$$

$$E_e = \frac{E_1 E_2}{E_1 + E_2}. \qquad (A17)$$

The result for this model is that the energy term in *Eq A1* becomes

$$S = \tfrac{1}{2} \left(\frac{P}{A}\right)^2 \left(\frac{2}{E_1} + \frac{1}{E_2}\right) \qquad (A18)$$

which seemingly can't be expressed in any simple form in terms of the observable properties of the material.

One possibly useful result obtains if the value of tan δ is taken as the maximum value found in a frequency sweep at each temperature. Then, for a peel angle of 90°

$$-\widetilde{\gamma} + \widetilde{P} + \widetilde{P}^2 = \tfrac{1}{2} \widetilde{P}^2 \left(\frac{1 + 3\tan\delta}{1 + \tan\delta}\right) \qquad (A19)$$

where

$$\widetilde{\gamma} = \gamma/E_e t \qquad (A20)$$

$$\widetilde{P} = P/AE_e \qquad (A21)$$

The solution of this quadratic is shown in *Fig. A3*, which demonstrates that the primary source of peel force is still the interfacial bonding strength γ.

The limiting forms of *Eq A19* are

$$\widetilde{P} = -1 + \sqrt{1 + 2\widetilde{\gamma}} \qquad (A22)$$

for low values of tan δ, and

$$\widetilde{P} = \widetilde{\gamma} \qquad (A23)$$

for high values.

As the reduced peel force is trivially dependent of the cross-sectional area and modulus of the peel, while the reduced work of adhesion is trivially dependent on modulus and thickness, the limiting expression of *Eq A23* is $P = w\gamma$. This is the same as the result in *Eq A11* for a peel angle of 90°, which is not surprising as a high loss tangent corresponds to a very high value of spring E_2, i.e., the Voigt element is recovered.

REFERENCES

1. A. L. Bisio and M. Xanthos, *How to Manage Plastic Waste, Technology and Market Opportunities*, Hanser Publishers, New York (1995).

2. R. J. Ehrig, *Plastics Recycling, Products and Processes*, Hanser Publishers, New York (1992).
3. E. H. Good, *Assoc. Rot. Molding*, Chicago (1992).
4. J. Ogando, *Plast. Tech.*, **38**, 43 (1992).
5. A. N. Gent and S. M. Lai, *J. Polym. Sci. B-Polym. Phy.*, **32**, 1543 (1994).
6. H. H. Shih and G. R. Hamed, *J. Appl. Polym. Sci.*, **63**, 333 (1997).
7. M. J. Loukis and N. Aravas, *J Adhesion*, **35**, 7 (1991).
8. K. Horiuchi and K. Sato, *J. Coat. Tech*, **63**, 55 (1991).
9. Y. Kano, S. Kawahara, and S. Akiyama, *J. Adhesion*, **42**, 25 (1993).
10. P. J. Flory, *Principles of Polymer Chemistry*, Cornell University Press, Ithaca, N.Y. (1953).
11. J. Brandup and E. H. Immergut, *Polymer Handbook*, Wiley, New York (1975).
12. S. P. Timoshenko and J. N. Goodier, *Theory of Elasticity*, McGraw-Hill, Inc., New York (1987).
13. J. D. Ferry, *Viscoelastic Properties of Polymers*, Wiley, New York (1980).
14. M. Chiang and H. Chai, *Int. J. Sol. Struct.*, **35**, 799 (1998).
15. R. Weinlein, PhD thesis, Technische Universitaet Berlin (1996).
16. H. Rumpf, *Kunststoffe*, **44**, 1954 (1993).
17. D. Mayerhauser, *Fortschritte in der Zerkleinerungstechnik insbesondere bei Schneidmühlen, in Verwerten von thermoplastischen, Kunststoffabfälle*, Düsseldorf (1979).
18. K. Leschonski, *Lehrstuhl fur mechanische Verfalmenstechmik*, April, 1981.
19. A. N. Gent and G. R. Hamed, *Polym. Eng. Sci.*, **17**, 462 (1977).
20. G. P. Anderson, K. L. DeVries, and M. L. Williams, *Exper. Mechanics*, **33**, 11 (1976).
21. J. A. Sauer and K. D. Pae, in *Introduction to Polymer Science and Technology: An SPE Textbook*, p. 301, H. S. Kaufmann and J. J. Falcetta, eds., Wiley-Interscience, New York (1977).